Electrophoresis

WILEY-VCH

ELECTROPHORESIS

RESEARCH ARTICLE

Lorenz Model for Chaos in Electrokinetic Instability

Prateek Gupta[1] | Supreet Singh Bahga[2]

[1]Department of Applied Mechanics, Indian Institute of Technology Delhi, New Delhi, India | [2]Department of Mechanical Engineering, Indian Institute of Technology Delhi, New Delhi, India

Correspondence: Supreet Singh Bahga (bahga@mech.iitd.ac.in)

Received: 11 September 2024 | **Revised:** 17 December 2024 | **Accepted:** 22 January 2025

Funding: This study was supported by the Science and Engineering Research Board, Government of India, under the Mathematical Research Impact Centric Support (MATRICS) scheme (Grant No. MTR/2022/000080).

Keywords: chaos | electrokinetic instability | nonlinear dynamics

ABSTRACT

We demonstrate that the Lorenz system of equations can approximate the nonlinear flow dynamics of the electrokinetic instability (EKI) in a microchannel driven by an electric field applied parallel to the diffusive interfaces separating the co-flowing centre and sheath streams with mismatched electrical conductivity. Using Galerkin projection, we show that the electrohydrodynamic flow equations can be approximated by the Lorenz equations in the limit of small conductivity difference between the flow streams. The derived dynamical model qualitatively captures the characteristics of EKI in both linear and nonlinear regimes, including the neutral stability criterion and alternating transitions between periodic and aperiodic states with increasing electric Rayleigh numbers. While not quantitatively precise, this simplified dynamical model provides valuable insights into the essential nonlinearities responsible for chaotic behaviour observed in EKI experiments.

1 | Introduction

Electrokinetic transport of ionic species and fluids is widely employed in microfluidic lab-on-a-chip devices for separation and preconcentration of charged species and control of fluid flow [1]. In many electrokinetic processes, conditions arise where electrical conductivity gradients are present in the bulk solution along with an externally applied electric field [2–4]. The application of an electric field through a solution with heterogeneous conductivity can lead to an accumulation of free charge in the bulk liquid. This free charge in the presence of an electric field leads to an electric body force on the fluid, which can drive an unstable electrohydrodynamic (EHD) flow above a threshold value of the electric field [2, 5, 6]. EHD instabilities can lead to undesirable sample dispersion in electrophoretic separation and preconcentration techniques [2, 7]. However, these instabilities can be leveraged for rapid micromixing in low Reynolds number flows [8].

EHD instabilities have been observed in various systems where conductivity gradients are generated by miscible or immiscible fluid layers having different conductivities [6]. Moreover, EHD instabilities have been reported for different configurations that differ in terms of the relative orientations of external electric field and conductivity gradient [6]. The current work deals with a well-known EHD instability in a cross-shaped microfluidic device that was originally reported by Shin et al. [9] and Posner and Santiago [10]. In this case, electro-osmotic flow (EOF) establishes a base-state flow with two sheath streams co-flowing with a miscible centre stream with different conductivity, as illustrated in Figure 1a. Therefore, the base state is characterized by an applied electric field parallel to the diffusive interfaces separating the streams of different conductivities. Beyond a critical value of the applied electric field, the flow destabilizes and exhibits sinuous or varicose disturbances of the centre stream, depending on whether the conductivity of the centre stream is higher or lower than that of sheath streams [10–12]. Figure 1b shows the experimental

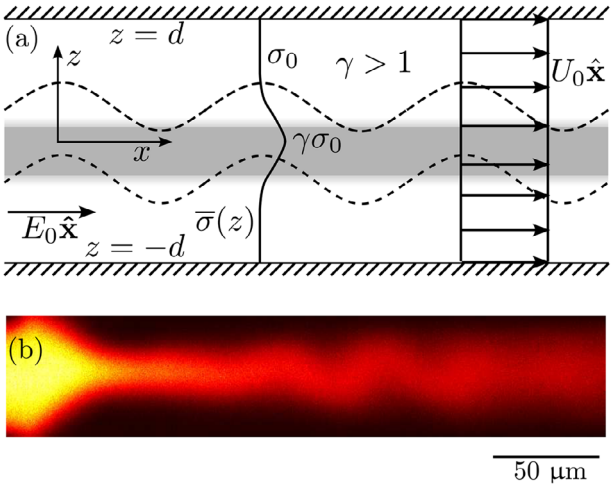

FIGURE 1 | Schematic and experimental visualization of EKI with co-flowing sheath and centre streams with mismatched electrical conductivities. (a) The schematic shows the base state wherein the electric field is applied parallel to the diffused interfaces separating the streams with unequal conductivities. When the centre stream has higher conductivity than the sheath streams ($\gamma > 1$), above a threshold electric field, the instability occurs in the form of a sinuous disturbance of the centre stream, shown in dashed lines. (b) Experimental snapshot of EKI, reproduced from Dubey et al. [11] showing the sinuous mode of instability.

visualization of the sinuous mode of the instability by Dubey et al. [11] that occurs when the centre stream has higher conductivity than the sheath stream. The flow instability results purely due to EHD coupling in the regions with conductivity gradients, while EOF establishes the base-state conductivity gradients and convects the disturbances downstream [13]. However, to emphasize the role of EOF, such instability is termed electrokinetic instability (EKI) [6]. The EKI corresponding to the base-state flow shown in Figure 1a is not only relevant for rapid micromixing but has also been observed in microchip electrophoretic processes. In particular, Dubey et al. [2] experimentally showed that the streamwise conductivity gradients in field-amplified sample stacking result in a recirculatory EOF that leads to an EKI similar to that depicted in Figure 1.

EKI in the flow configuration shown in Figure 1 has also been shown to exhibit chaotic dynamics at high electric fields despite a low Reynolds number [14]. Specifically, experimental observations of Posner and Santiago [14] show that upon a sequential increase in the electric field, the flow transitions from a steady to a periodic state, followed by an aperiodic chaotic state. Interestingly, Posner and Santiago also observed that the flow exhibits multiple periodic to aperiodic transitions upon increasing the applied electric field. Similar electrokinetic flows have also been shown to exhibit turbulent flow-type chaotic characteristics at high electric fields [15]. Besides microchannel flows, chaotic EHD flows have also been observed in various other systems, such as in nematic liquid crystals [16] and near ion-selective membranes [17].

Despite the experimental observations of the chaotic behaviour of EKI at high electric fields [14], the theoretical basis underlying the transition to chaos in EKI is poorly understood. In contrast, various physical and chemical systems that exhibit chaotic behaviour have been qualitatively described using simplified dynamical system models [18]. Notable among such dynamical models is the Lorenz system of ordinary differential equations, which was presented by Lorenz [19] in 1963, to qualitatively explain the transition to chaos in Rayleigh–Bénard convection, driven by a thermal gradient. The seminal work of Lorenz laid the foundations of chaos theory, showing that completely deterministic systems can lead to unpredictable, chaotic behaviour over long periods of time, owing to their sensitivity to initial conditions. The chaotic dynamics of various other systems, such as electrical circuits, lasers and chemical reactions, can also be described using the Lorenz equations and similar nonlinear dynamical models [18, 20]. However, to date, a simplified dynamical model describing the transition to chaos in EKI has not been proposed.

Recently, Guan et al. [21] presented a reduced-order model of EHD flow with unipolar charge injection using a data-driven framework for model identification from direct numerical simulation (DNS) data. The dynamical model of Guan et al. consists of three nonlinear, first-order differential equations for the time-varying amplitudes of dominant modes of flow obtained using proper orthogonal decomposition. However, their dynamical model for capturing the chaotic dynamics of EHD flow is limited to the single set of operational conditions at which the DNS was performed. Consequently, the model cannot be used to capture the transition to chaos upon increasing the electric field.

In this paper, we follow Lorenz's approach [19] of using Galerkin projection of the governing equations onto a small set of basis functions to derive a simple dynamical model for EKI. We show that the dynamics of EKI, depicted in Figure 1, can be described using the Lorenz equations in the limit of small conductivity difference between the centre and sheath streams. The derived dynamical model for EKI qualitatively captures the dynamics of EKI at varying operating conditions, described by the electric Rayleigh number. Specifically, the model predicts a neutral stability criterion for the transition between stable and unstable states that agrees qualitatively with experimental observations and the predictions of detailed linear stability analysis. Interestingly, the dynamical model also captures the experimentally observed alternating transitions between periodic and aperiodic states upon increasing the electric Rayleigh number. Moreover, the dynamical model for EKI describes the nonlinearities underlying the transition to chaos in EKI. Because the properties of the Lorenz equations have been extensively studied in the literature [20, 22], in this paper, we focus primarily on deriving the Lorenz equations from the governing equations for EKI and showing that their predictions agree qualitatively with experimental observations.

2 | Mathematical Modelling

We consider the electric-field driven instability of two-dimensional, planar, co-flowing centre and sheath streams between walls at $z = \pm d$, as shown in Figure 1. The channel walls extend infinitely in the x and y directions. An external electric field $E_0\hat{\mathbf{x}}$ is applied along the x-direction, which drives a uniform EOF with velocity $U_0\hat{\mathbf{x}}$ due to a thin electrical double layer (EDL) at the walls. The centre and sheath stream fluids are

considered binary electrolytes of the same salt but with different concentrations. In particular, we consider the case where the centre stream has higher conductivity than the sheath streams. These streams are convected downstream by the EOF. The convection and diffusion of the salt ions in the centre and sheath streams govern the base state conductivity distribution.

Typically, EKI experiments are performed in microchannels with a width and depth of $\mathcal{O}$(10–100 μm) and length of $\mathcal{O}$(1 cm). The electrical conductivity of the electrolyte solutions is $\mathcal{O}$(0.05–0.5 S m^{-1}) corresponding to salt concentrations of $\mathcal{O}$(1–10 mM). For such dilute electrolytes, the viscosity, density and electrical permittivity can be assumed to be those of pure water. EKI is observed at an axial electric field $E_0\hat{\mathbf{x}}$ of $\mathcal{O}$(10 kV m^{-1}) [10, 11]. The EOF at these electric fields is $\mathcal{O}$(1 mm s^{-1}). For a typical diffusivity of salt ions of $\mathcal{O}(10^{-9}$ m^2 s$^{-1})$, the Peclet number $Pe = U_0 d/D$ for convection–diffusion of conductivity field is at least $\mathcal{O}$(10).

2.1 | Governing Equations

The governing equations for modelling EKI are based on the Ohmic model [13], which is derived from the Nernst–Plank equations for a symmetric binary electrolyte, assuming instantaneous charge relaxation and electroneutrality. The Ohmic model is given by the following equations:

$$\nabla \cdot \mathbf{u} = 0, \tag{1}$$

$$\rho\frac{\partial \mathbf{u}}{\partial t} + \rho\mathbf{u}\cdot\nabla\mathbf{u} = -\nabla p + \eta\nabla^2\mathbf{u} + \mathbf{E}\nabla\cdot(\epsilon\mathbf{E}), \tag{2}$$

$$\nabla\cdot(\sigma\mathbf{E}) = 0, \tag{3}$$

$$\nabla\times\mathbf{E} = \mathbf{0}, \tag{4}$$

$$\frac{\partial\sigma}{\partial t} + \mathbf{u}\cdot\nabla\sigma = D\nabla^2\sigma. \tag{5}$$

Here, $\mathbf{u}$ denotes the flow velocity, $\mathbf{E}$ the local electric field, p the pressure, σ the electrical conductivity, ϵ the permittivity (assumed to be constant), ρ and η, respectively, denote the density and dynamic viscosity of the liquid and D denotes the effective diffusivity that depends on the diffusivities of the cations and the anions as $D = 2D_+D_-/(D_+ + D_-)$ [13].

Note that for EHD flow in aqueous electrolytes on a millimetre or shorter length scales, the convection current is negligible compared to the conduction current, as the electrical relaxation time is significantly smaller than the convection timescale [23]. Therefore, the convection current is ignored in Equation (3) for current continuity. Moreover, as discussed by Saville [23], the electrostatic assumption applies for EHD flows because the timescale for the magnetic phenomenon is significantly smaller than the electrical relaxation time. Because the electric field is irrotational, the electric field can be expressed in terms of an electric potential ϕ as $\mathbf{E} = -\nabla\phi$. Equations (1)–(5) describe the EHD flow of a symmetric binary electrolyte with diffusive conductivity gradients. High-fidelity numerical simulations of EKI based on these equations by Li et al. [24] and their agreement with experimental data suggest that Equations (1)–(5) accurately model EKI.

2.2 | Base State

The base-state conductivity distribution $\overline{\sigma}$ is considered to be steady, for which the conductivity transport equation, Equation (5) simplifies to

$$U_0\frac{\partial\overline{\sigma}}{\partial x} = D\nabla^2\overline{\sigma}. \tag{6}$$

In the current case, $Pe = U_0 d/D \sim \mathcal{O}(10)$ and hence the ion transport is convection-dominated. Moreover, for slender channels, the axial diffusion is negligible compared with spanwise diffusion. Consequently, the base-state conductivity varies slowly along the axial direction. Therefore, we approximate the solution of Equation (6) as

$$\frac{\overline{\sigma}(z)}{\sigma_0} = 1 + (\gamma - 1)\exp\left(-\frac{z^2}{2\delta^2}\right), \tag{7}$$

with no axial conductivity variation. Here, σ_0 is the conductivity of the sheath streams and γ is the ratio of conductivities of the centre and sheath streams. That is, in the base state, the electric field is parallel to the two diffusive interfaces separating the flow streams. For our calculations, we consider $\delta = d/4$, which corresponds to vanishingly small conductivity gradients near the domain boundaries $z = \pm d$.

2.3 | Dimensionless Governing Equations

We shall use dimensionless variables for our analysis, for which we nondimensionalize the governing equations (Equations 1–5), using the following reference scales:

$$[x, y, z] = d, \quad [\mathbf{E}] = E_0, \quad [\boldsymbol{\phi}] = E_0 d, \quad [\mathbf{u}] = \frac{D}{d},$$
$$[t] = \frac{d^2}{D}, \quad [p] = \frac{\eta D}{d^2}, \quad [\sigma] = \sigma_0. \tag{8}$$

We note that typically, to model an EKI, the reference scale for velocity is taken to be the electroviscous velocity scale $U_{ev} = \epsilon E_0^2 d/\eta$, which is obtained by balancing the electric body force and viscous stresses [13, 25]. However, here, we have chosen the D/d as the velocity scale to draw an analogy with the analysis of Rayleigh–Bénard convection wherein the velocity scale is taken as κ/d, κ being the thermal diffusivity of the fluid.

Upon nondimensionalizing the governing equations (Equations 1–5), using these reference scales and using $\mathbf{E} = -\nabla\phi$ we obtain the following set of dimensionless governing equations:

$$\nabla\cdot\mathbf{u} = 0, \tag{9}$$

$$Sc^{-1}\left[\frac{\partial\mathbf{u}}{\partial t} + \mathbf{u}\cdot\nabla\mathbf{u}\right] = -\nabla p + \nabla^2\mathbf{u} + Ra_e\left(\nabla^2\phi\right)\nabla\phi, \tag{10}$$

$$\nabla\cdot(\sigma\nabla\phi) = 0, \tag{11}$$

$$\frac{\partial\sigma}{\partial t} + \mathbf{u}\cdot\nabla\sigma = \nabla^2\sigma. \tag{12}$$

Here, $Ra_e = \epsilon E_0^2 d^2/(\eta D)$ is the electric Rayleigh number and $Sc = \eta/(\rho D)$ is the Schmidt number. In Equations (9)–(12), $\mathbf{u}$, p, ϕ and σ denote the dimensionless velocity, pressure, electric potential and conductivity, respectively. Henceforth, we use only the dimensionless variables in our analysis.

The electric Rayleigh number Ra_e in the momentum equation (Equation 10) is the main dimensionless parameter that can be varied to induce EKI. The electric Rayleigh number is the ratio of timescales associated with the diffusion of conductivity ($\tau_d = d^2/D$) and the convection due to electroviscous flow ($\tau_{ev} = d/U_{ev} = \eta/(\epsilon E_0^2)$). That is, $Ra_e = \tau_d/\tau_{ev}$. EKI sets in when the destabilizing electroviscous flow stretches the conductivity gradients faster than the diffusion of the conductivity gradients, that is, $\tau_{ev} \ll \tau_d$. Therefore, increasing Ra_e by applying a stronger electric field results in a transition from stable to unstable flow [10, 11]. Note that a higher value of Ra_e corresponds to a stronger electric body force in the nondimensionalized momentum equation (Equation 10).

2.4 | Equations for Two-Dimensional Disturbances

In the base state, illustrated in Figure 1, the dimensionless velocity, electric potential and pressure are given by

$$\overline{\mathbf{u}} = U\hat{\mathbf{x}}, \quad \overline{\phi} = -x, \quad \overline{p} = 0, \tag{13}$$

where $U = U_0 d/D$. The base state conductivity $\overline{\sigma}$ upon nondimensionalizing equation (7), is given by

$$\overline{\sigma}(z) = 1 + (\gamma - 1)\exp\left(-8z^2\right). \tag{14}$$

Note that there is no free charge in the base state because, in the base state, the applied electric field is parallel to the diffusive interfaces separating the streams with mismatched conductivities. Because the base-state flow velocity is uniform, it is convenient to model the instability in the reference frame translating at the base-state velocity $U\hat{\mathbf{x}}$. Henceforth, we denote x to be the axial coordinate in the reference frame translating at the base-state velocity $U\hat{\mathbf{x}}$. In this reference frame, the base-state velocity is $\overline{\mathbf{u}} = \mathbf{0}$.

To derive the dynamical model for EKI, we assume a two-dimensional flow in the $x-z$ plane with velocity field $\mathbf{u} = u(x,z,t)\hat{\mathbf{x}} + w(x,z,t)\hat{\mathbf{z}}$. To model the behaviour of two-dimensional disturbances over the base state, we decompose ϕ and σ in terms of their base state and perturbation (denoted by primes) values,

$$\phi = \overline{\phi} + \phi' \quad \text{and} \quad \sigma = \overline{\sigma} + \sigma'. \tag{15}$$

Note that the base-state values of velocity in the reference frame translating at $U\hat{\mathbf{x}}$ and pressure are zero; hence, $\mathbf{u}$ and p represent the perturbation velocity and pressure, respectively. Upon substituting these variables in the dimensionless governing equations (Equations 9–12), we obtain the following governing equations for perturbation variables,

$$\nabla \cdot \mathbf{u} = 0, \tag{16}$$

$$Sc^{-1}\left[\frac{\partial \mathbf{u}}{\partial t} + \mathbf{u}\cdot\nabla\mathbf{u}\right] = -\nabla p + \nabla^2\mathbf{u} + Ra_e\nabla^2\phi'(-\hat{\mathbf{x}} + \nabla\phi'). \tag{17}$$

$$\nabla\cdot\left((\overline{\sigma}+\sigma')\nabla\phi'\right) - \frac{\partial\sigma'}{\partial x} = 0, \tag{18}$$

$$\frac{\partial\sigma'}{\partial t} + u\frac{\partial\sigma'}{\partial x} + w\frac{\partial\sigma'}{\partial z} = -w\frac{d\overline{\sigma}}{dz} + \nabla^2\sigma'. \tag{19}$$

Here $\nabla^2 \equiv \partial^2/\partial x^2 + \partial^2/\partial z^2$. Note that Equations (16)–(19) account for all the nonlinearities in the governing equations (Equations 9–12). The only assumption made here is that, while deriving Equation (19), we have assumed the base-state conductivity field $\overline{\sigma}$ to approximately satisfy Equation (6).

Next, to derive an approximate dynamical model for EKI, we assume that the difference between the centre and sheath stream conductivities is small, that is, $|\gamma - 1| \ll 1$. In this limit, Equation (18) can be simplified by assuming $\sigma' \ll \overline{\sigma}$ and $\overline{\sigma} \approx 1$ from Equation (14). Therefore, Equation (18) simplifies to

$$\nabla^2\phi' = \frac{\partial\sigma'}{\partial x}. \tag{20}$$

That is, the free charge density (nondimensionalized by $\epsilon E_0/d$), $\rho_f = -\nabla^2\phi = -\partial\sigma'/\partial x$ depends only on the axial conductivity gradients.

To simplify the momentum equation (Equation 17), we express the x and z components of velocity in terms of a streamfunction $\psi(x,z,t)$ as

$$u = \frac{\partial\psi}{\partial z}, \quad w = -\frac{\partial\psi}{\partial x}, \tag{21}$$

which by definition satisfies the continuity equation (Equation 16). We then eliminate pressure from the momentum equation by taking the curl of Equation (17) to get

$$Sc^{-1}\left(\frac{\partial}{\partial t} + \frac{\partial\psi}{\partial z}\frac{\partial}{\partial x} - \frac{\partial\psi}{\partial x}\frac{\partial}{\partial z}\right)\nabla^2\psi = \nabla^4\psi + Ra_e\left(-\frac{\partial}{\partial z} + \frac{\partial\phi'}{\partial x}\frac{\partial}{\partial z} - \frac{\partial\phi'}{\partial z}\frac{\partial}{\partial x}\right)\nabla^2\phi'. \tag{22}$$

The convection–diffusion equation for electrical conductivity perturbation (Equation 19) can be expressed in terms of the streamfunction as

$$\frac{\partial\sigma'}{\partial t} + \frac{\partial\psi}{\partial z}\frac{\partial\sigma'}{\partial x} - \frac{\partial\psi}{\partial x}\frac{\partial\sigma'}{\partial z} = \frac{\partial\psi}{\partial x}\frac{\mathrm{d}\overline{\sigma}}{\mathrm{d}z} + \nabla^2\sigma'. \tag{23}$$

Equations (20), (22) and (23) are the necessary governing equations for ϕ', ψ and σ', which we shall simplify even further using the Galerkin method to derive the dynamical model for EKI.

2.5 | Boundary Conditions

To solve the governing equations (Equations 20, 22, and 23) at each boundary ($z = \pm 1$), we require one boundary condition for ϕ' and σ' and two boundary conditions for ψ. The boundary

condition for the velocity at an impenetrable wall within EDL is given by the electro-osmotic slip boundary condition. However, if the walls are sufficiently far from the conductivity gradients, the disturbances in the electric field and velocity near the walls are small, and the shear stress at the walls can be assumed to be negligible. Therefore, we consider the boundaries at $z = \pm 1$ to be impenetrable and stress-free [26], as described by

$$\psi = \frac{\partial^2 \psi}{\partial z^2} = 0 \quad \text{at} \quad z = \pm 1. \tag{24}$$

A similar boundary condition was used by Chen et al. [13] for the stability analysis of EKI. Though approximate, the stress-free boundary condition at the channel walls helps isolate the effect of destabilizing electroviscous flow on chaotic convection from EOF, as the latter is primarily responsible for downstream convection of disturbances and not destabilizing the flow [13].

The boundary condition for electric potential can be obtained by noting that the electric field normal to the boundaries at $z = \pm 1$ vanishes in the thin EDL limit. Also, no mass transfer occurs across the boundaries at $z = \pm 1$. Consequently, electric potential ϕ and conductivity σ obey homogeneous Neumann boundary conditions,

$$\frac{\partial \sigma'}{\partial z} = 0 \text{ and } \quad \frac{\partial \phi'}{\partial z} = 0 \quad \text{at} \quad z = \pm 1. \tag{25}$$

2.6 | Derivation of the Lorenz Model for EKI

We use the Galerkin method to derive a dynamical model for EKI. In particular, we limit the description of the streamfunction ψ using a Galerkin expansion with a single term,

$$\psi(x, z, t) = \psi_1(t) \cos\left(\frac{\pi z}{2}\right) \sin(kx), \tag{26}$$

where k is the wavelength of the disturbance. This form of streamfunction satisfies the boundary conditions given by Equation (24). Next, we consider the following Galerkin expansion for the conductivity perturbation σ':

$$\sigma'(x, z, t) = \sigma_1(t) \sin\left(\frac{\pi z}{2}\right) \cos(kx) + \sigma_2(t) \cos(\pi z). \tag{27}$$

This form for σ' satisfies the homogeneous Neumann boundary condition (Equation 25). Note that the second term in the expansion for σ', which is independent of x, is necessary to incorporate some nonlinearities of the system. Upon substituting the Galerkin expansion for σ' in Equation (20), we note that ϕ' is given by

$$\phi'(x, z, t) = \frac{k}{q^2} \sigma_1(t) \sin\left(\frac{\pi z}{2}\right) \sin(kx), \text{ where } q^2 = \frac{\pi^2}{4} + k^2, \tag{28}$$

which satisfies the boundary condition given by Equation (20). Upon substituting the expressions for ψ and ϕ' in Equation (22), we obtain,

$$Sc^{-1} \frac{d\psi_1}{dt} = -q^2 \psi_1 - \frac{k\pi}{2q^2} Ra_e \sigma_1. \tag{29}$$

Interestingly, the nonlinear terms of inertia and body force in Equation (22) drop out and we obtain a first-order linear differential equation for ψ_1.

Next, we substitute the expansions for ψ and σ' given by Equations (26) and (27) in the convection–diffusion equation (Equation 23) for σ'. The nonlinear term $\psi_z \sigma'_x - \psi_x \sigma'_z$ in Equation (23) is equal to

$$\frac{\partial \psi}{\partial z}\frac{\partial \sigma'}{\partial x} - \frac{\partial \psi}{\partial x}\frac{\partial \sigma'}{\partial z} = \frac{k\pi}{2}\psi_1 \left[-\frac{\sigma_1}{2}(\cos(2kx) + \cos(\pi z)) + \sigma_2 \cos(kx)\left(\sin\left(\frac{\pi z}{2}\right) + \sin\left(\frac{3\pi z}{2}\right)\right)\right]. \tag{30}$$

Using this expression and upon substituting the expansions for ψ and σ' in Equation (23) yields

$$\begin{aligned} &\cos(\pi z)\left[\frac{d\sigma_2}{dt} - \frac{\pi k}{4}\psi_1\sigma_1 + \pi^2\sigma_2\right] \\ &\quad + \cos(kx)\sin\left(\frac{\pi z}{2}\right)\left[\frac{d\sigma_1}{dt} + \frac{\pi k}{2}\psi_1\sigma_2 + q^2\sigma_1\right] \\ &= k\psi_1 \cos\left(\frac{\pi z}{2}\right)\frac{d\overline{\sigma}}{dz}\cos(kx) \\ &\quad - \frac{k\pi}{2}\psi_1\left[-\frac{\sigma_1}{2}\cos(2kx) + \sigma_2\cos(kx)\sin\left(\frac{3\pi z}{2}\right)\right]. \end{aligned} \tag{31}$$

Comparing the various terms in Equation (31) yields a nonconvective solution ($\psi_1 = 0$) if equality of all terms is desired. Therefore, instead of enforcing exact equality, we use the orthogonality of functions 1, $\sin(\pi z/2)$, $\cos(\pi z)$ and $\sin(3\pi z/2)$ over the interval $-1 \le z \le 1$ to obtain ordinary differential equations for σ_1 and σ_2.

To obtain an ordinary differential equation for σ_1, we multiply both sides of Equation (31) with $\sin(\pi z/2)$ and integrate over $-1 \le z \le 1$ to get

$$\frac{d\sigma_1}{dt} = -kI\psi_1 - \frac{\pi k}{2}\psi_1\sigma_2 - q^2\sigma_1, \tag{32}$$

where I is a definite integral defined as,

$$I = -\int_{-1}^{1} \frac{d\overline{\sigma}}{dz} \cos\left(\frac{\pi z}{2}\right) \sin\left(\frac{\pi z}{2}\right) dz. \tag{33}$$

Note that for the base-state conductivity $\overline{\sigma}$ given by Equation (14), the above integral can be approximated as $I = 0.723(\gamma - 1)$. That is, for the case which we consider here with the centre stream having higher conductivity than the sheath streams ($\gamma > 1$), the integral $I > 0$.

Similarly, the ordinary differential equation for σ_2 is obtained by multiplying both sides of Equation (31) with $\cos(\pi z)$ and integrating over $-1 \le z \le 1$, which yields

$$\frac{d\sigma_2}{dt} = \frac{\pi k}{4}\psi_1\sigma_1 - \pi^2\sigma_2. \tag{34}$$

Equations (29), (32) and (34) form a system of nonlinear ordinary differential equations for the amplitudes ψ_1, σ_1 and σ_2. Lastly, we express this system of equations in terms of the standard Lorenz equations by using the following change of variables:

$$T = q^2 t,\ X = -\frac{\pi k}{2\sqrt{2}q^2}\psi_1,\ Y = \frac{\pi^2 k^2 Ra_e}{4\sqrt{2}q^6}\sigma_1,\ Z = -\frac{\pi^2 k^2 Ra_e}{4q^6}\sigma_2, \tag{35}$$

where $q^2 = \pi^2/4 + k^2$. Using the transformed variables Equations (29), (32) and (34) can be expressed in the form of the Lorenz equations,

$$\frac{dX}{dT} = Sc(Y - X), \tag{36a}$$

$$\frac{dY}{dT} = -XZ + rX - Y, \tag{36b}$$

$$\frac{dZ}{dT} = XY - bZ. \tag{36c}$$

Here, Sc is the Schmidt number and r and b are parameters defined as

$$r = \frac{\pi I k^2}{2q^6} Ra_e, \quad \text{and} \quad b = \frac{\pi^2}{q^2}, \tag{37}$$

where $I = 0.723(\gamma - 1)$. Note that r depends on the electric Rayleigh number Ra_e and the conductivity ratio γ. Therefore, a given value of r can correspond to different combinations of Ra_e and $\gamma > 1$.

The above derivation of the Lorenz equations for EKI is based on a drastic simplification of the governing equations for EHD flow using a few terms in the Galerkin method. Therefore, the Lorenz model described by Equation (36) can, at best, describe only the qualitative characteristics of EKI. Also, we note that Equation (36a) that corresponds to the momentum equation is a linear differential equation. Specifically, the nonlinear inertial terms in the momentum equation (Equation 22) drop out during the application of the Galerkin method. The model has only two nonlinear terms in Equations (36b) and (36c) that correspond to the convection of the conductivity field. This indicates that the chaotic dynamics of EKI are a result of chaotic convection of the conductivity field rather than nonlinearity due to flow inertia. For the same reason, experiments show that EKI exhibits chaos despite a low Reynolds number [14].

3 | Results and Discussion

We have shown that the dynamics of EKI can be qualitatively described using the Lorenz equations given by Equation (36). The properties of the Lorenz equations and their solutions for varying parameter values are well documented in excellent texts such as those by Strogatz [20], Bergé et al. [18] and Sparrow [22]. In this section, we summarize the predictions of the Lorenz equations, particularly in the context of EKI, to show the model predictions qualitatively describe the reported experimental observations.

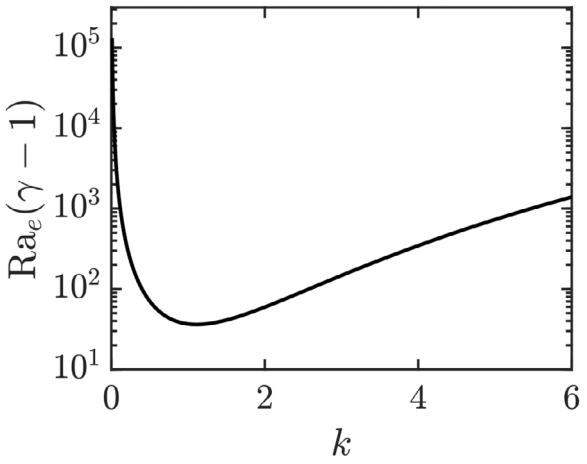

FIGURE 2 | Neutral stability curve for EKI, given by Equation (38). The minimum value of Ra_e is attained at $k = \pi/(2\sqrt{2}) \approx 1.11$, at which $Ra_{e,\mathrm{cr}}(\gamma - 1) = 36.18$.

Note that, typically, Lorenz equations are solved for $Sc = 10$, which in the context of thermal convection is the Prandtl number. However, for a typical EKI experiment with aqueous electrolytes, $Sc = 1000$ corresponding to $\eta = 10^{-3}$ Pa s, $\rho = 1000$ kg m^{-3} and $D = 10^{-9}$ m^2 s^{-1}. The large value of $Sc = 1000$ for EKI makes the Lorenz model significantly more dissipative compared with the standard case with $Sc = 10$. For our discussion, we take $b = 8/3$, which, as shown later in Section 3.1, corresponds to the wavenumber of the least stable disturbance at the onset of EKI. The parameter r, defined by Equation (37), depends on the electric Rayleigh number Ra_e, and hence it governs the onset of EKI and transition to chaos. Below, we discuss the behaviour of solutions of the Lorenz model (Equation 36) for varying values of r.

3.1 | Onset of EKI

The Lorenz system of equations has a fixed point at the origin $(X, Y, Z) = (0, 0, 0)$, which corresponds to the base state flow with no disturbances. Specifically, the origin is globally stable for $r < 1$ [20]. That is, at low Rayleigh numbers corresponding to $r < 1$, any perturbation over the base state flow vanishes over time. For $1 < r < r_H = Sc(Sc + b + 3)/(Sc - b - 1)$, the system has a pair of symmetric, linearly stable, fixed points $X = Y = \pm\sqrt{b(r-1)}$, $Z = r - 1$, denoted as C^+ and C^- [20]. In the context of EKI, these states correspond to stationary convection rolls superposed on the uniform base state EOF. Note that for $Sc = 1000$, $r_H \approx 1000$.

Because the destabilizing convective rolls start appearing in the flow beyond $r = 1$, this marks the condition for the onset of EKI. Therefore, setting $r = 1$ in Equation (37), while noting that $I \approx 0.723(\gamma - 1)$ and $q^2 = \pi^2/4 + k^2$ yields the threshold electric Rayleigh number for the onset of EKI,

$$Ra_e(\gamma - 1) = \frac{2}{0.723\pi}\frac{(\pi^2/4 + k^2)^3}{k^2}. \tag{38}$$

This equation suggests that a smaller conductivity mismatch between centre and sheath streams requires a higher threshold Ra_e to induce EKI. Figure 2 shows the neutral stability curve given by Equation (38). Despite the drastic simplifications made to

arrive at the Lorenz equations for EKI, the neutral stability curve shown in Figure 2 is qualitatively similar to the neutral curves obtained using linear stability analysis for EHD instabilities in various configurations [27–29]. In particular, the Lorenz equations (Equation 36) predict that the instability is characterized by a stationary mode (C^+ and C^- fixed points) superposed on the base-state flow. That is, when r is increased beyond the threshold value of $r = 1$, EKI is characterized by stationary convection cells in the frame of reference translating with the uniform base state flow, which is consistent with the predictions based on linear stability analysis [27]. These convection cells superposed on base state EOF appear as periodic disturbances in a stationary reference frame, as observed in reported EKI experiments [10, 11].

The critical value of Ra_e given by Equation (38), occurs at $k^2 = \pi^2/8$ at which the electric Rayleigh number attains a minimum value of

$$Ra_{e,\mathrm{cr}} = \frac{36.18}{\gamma - 1}. \tag{39}$$

To compare this value with experiments, we consider the parametric experimental study of Posner and Santiago [10] wherein EKI experiments were performed in $w = 50$ μm wide and $h = 20$ μm deep D-shaped glass microchannels. Based on an extensive set of experiments for varying ratios of centre-to-sheath stream conductivities (γ), Posner and Santiago [10] estimated that the critical electric field for the onset of EKI, for the case of $\gamma > 1$, is given by

$$\frac{\epsilon E_{\mathrm{cr}}^2 h^2}{\eta D}\left(\frac{\gamma - 1}{\gamma}\right) = 205. \tag{40}$$

Expressing the above relation in terms of the half-depth of the microchannel, $d = h/2$, yields

$$Ra_{e,\mathrm{cr}} = 51.25\left(\frac{\gamma}{\gamma - 1}\right). \tag{41}$$

For a small difference between centre and sheath stream conductivities, $\gamma \approx 1$, which we have assumed while deriving the Lorenz equations, the theoretical critical Ra_e given by Equation (39) agrees well with the experimentally estimated value given by Equation (41). Note that the electric Rayleigh number for the experiments given by Equation (41) is defined in terms of the channel half-depth because, in the shallow microchannels used in the experiments, the gradients in the depth direction are much larger than those in the width direction. On the other hand, Ra_e in our mathematical model is based on the channel half-width owing to the two-dimensional flow configuration. Lastly, we note that at the theoretically predicted critical state corresponding to $k^2 = \pi^2/8$, the parameter $b = \pi^2/q^2$ in the Lorenz equations has a value of $b = 8/3$. Therefore, hereafter, for all our calculations, we use $b = 8/3$.

3.2 | Chaotic Motion

The Lorenz equations (Equation 36) are known to exhibit aperiodic, chaotic solutions beyond $r = r_H = Sc(Sc + b + 3)/(Sc - b - 1)$ [20]. For $Sc = 1000$ and $b = 8/3$ in the current case, $r_H \approx 1000$.

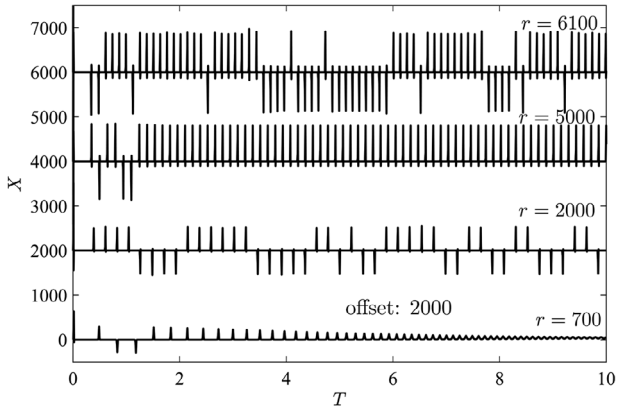

FIGURE 3 | Time evolution of X for varying values of parameter r obtained by numerical integration of Lorenz equations (Equation 36). For these calculations, we used $Sc = 1000$ and $b = 8/3$. Upon sequentially increasing r, the system exhibits chaotic behaviour at $r = 2000$ and 6100. However, the Lorenz equations predict periodic oscillations at an intermediate value of $r = 5000$. The time series of X are offset by a value of 2000 for plotting purposes.

Moreover, the Lorenz equations are known to predict back-and-forth transitions between periodic to aperiodic solutions upon sequentially increasing r [20]. Similar back-and-forth transitions between periodic and aperiodic states have been observed in EKI experiments by Posner and Santiago [14] upon increasing the electric Rayleigh number. To demonstrate this behaviour, we numerically integrated the Lorenz equations (Equation 36) for varying values of r for $Sc = 1000$ and $b = 8/3$. For all our calculations, we used the initial conditions $(X, Y, Z) = (1, 1, 1)$.

Figure 3 shows the temporal evolution of X for varying values of parameter r. For plotting purposes, the time series of X are sequentially offset by a value of 2000. For $r = 700 < r_H$, the perturbations decay over time and X approaches the C^+ fixed point $X = \sqrt{b(r-1)}$. For $r = 2000$, the Lorenz equations yield an aperiodic, chaotic solution characterized by irregular, non-repeating oscillations. At $r = 5000$, the system undergoes initial transients before exhibiting periodic oscillations. At an even higher value of $r = 6100$, the Lorenz equations for EKI again predict a chaotic behaviour. Such predictions of back-and-forth transition from regular to irregular, chaotic flow are in qualitative agreement with EKI experiments of Posner and Santiago [14].

Next, to visualize the periodic limit cycles and the chaotic states (attractor), in Figure 4, we plot the projection of computed trajectories on the $X - Y$ plane for varying values of r. In Figure 4, we have omitted the initial transients to visualize the long-term model predictions. Figure 4a shows the chaotic trajectories of the Lorenz equations on the $X - Y$ phase portrait for $r = 2000$. The phase portrait shows that the nonrepeating trajectories are localized in a complex-shaped region, which is characteristic of chaotic behaviour [20]. The phase portrait for $r = 5000$, shown in Figure 4b, shows that the trajectories follow a limit cycle, corresponding to the periodic solution shown in Figure 3. At a slightly higher value of $r = 5500$, the limit cycle consists of two closely spaced loops in the $X - Y$ phase portrait, as shown in Figure 4c. This indicates that the system takes

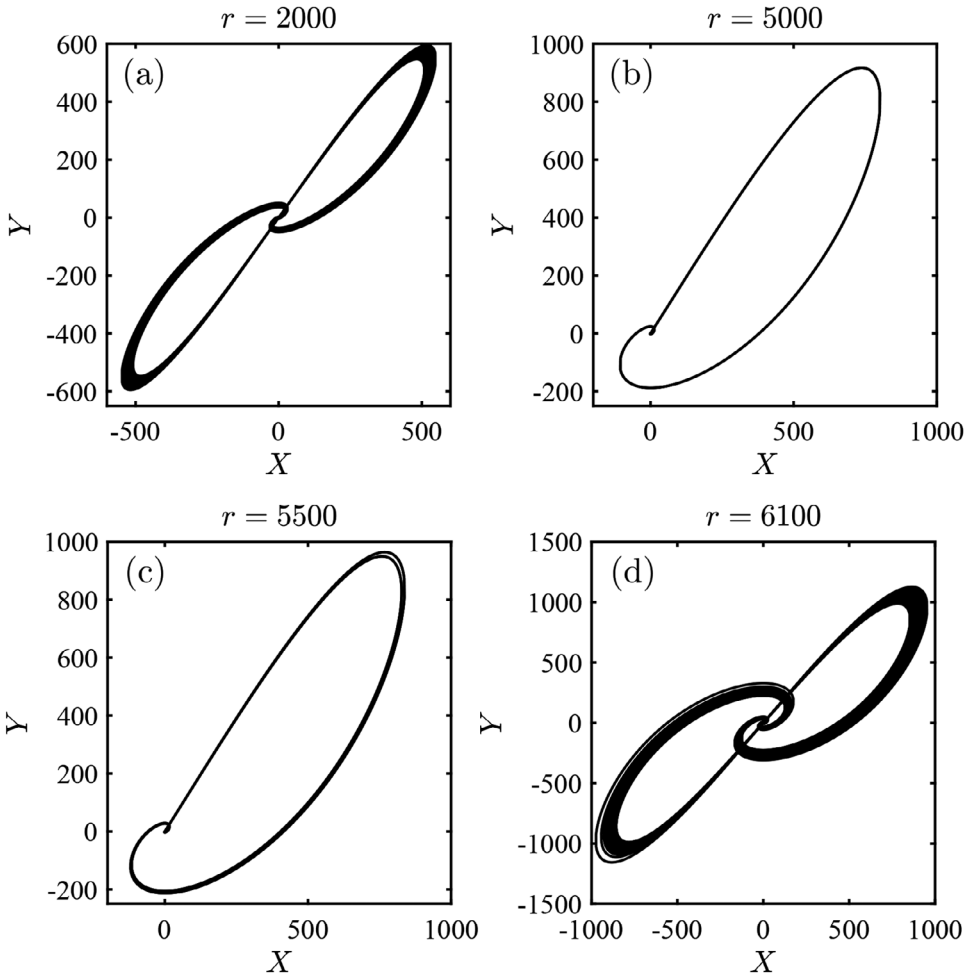

FIGURE 4 | The computed trajectories for Lorenz equations for EKI (Equation 36) for varying values of r for $Sc = 1000$ and $b = 8/3$. The phase portraits (a) and (d) show chaotic behaviour at $r = 2000$ and 6100, respectively. (b) shows a limit cycle at $r = 5000$, and (c) shows period-doubling behaviour at $r = 5500$.

approximately twice as long to return to the same state, resulting in a period-doubling behaviour. We note that the experiments of Posner and Santiago [10, 14] also showed such periodic doubling bifurcations. Lastly, Figure 4d shows chaotic behaviour upon further increasing r to 6100. We note that the shape of the chaotic attractor in the current case differs from the typical butterfly-shaped attractor [19, 20], because for EKI $Sc = 1000$ instead of the typical value of $Sc = 10$ used in the Lorenz equations for thermal convection. At large values of Sc, the Lorenz system of equations is even more dissipative, causing the trajectories to be tightly wound around the attractors, as shown in Figure 4a,d. Overall, Figures 3 and 4 show that the Lorenz equations for EKI (Equation 36) qualitatively capture the essential nonlinear characteristics of EKI, particularly the alternating periodic-chaotic behaviour at large values of electric Rayleigh number [14].

4 | Concluding Remarks

We have described the nonlinear dynamics of EKI in a microchannel driven by an electric field applied parallel to the diffusive interfaces separating co-flowing centre and sheath streams with mismatched electrical conductivity. In particular, we have shown that the Lorenz system of equations can approximate the dynamics of EKI in the limit of small conductivity difference between the centre and sheath streams. To this end, we used Galerkin projection of the equations governing EHD flow onto a small set of basis functions to show that the resulting dynamical model is identical to the Lorenz equations.

We also showed that the derived Lorenz equations qualitatively describe the various characteristics of EKI in the linear and nonlinear regimes. Despite the drastic simplifications made while deriving the dynamical model for EKI, the model yields a neutral stability criterion for the onset of instability that agrees qualitatively with the experimental observations and the predictions of detailed linear stability analysis. Moreover, the dynamical model also captures the alternating transitions between periodic and aperiodic states upon increasing the electric Rayleigh number. In summary, the Lorenz equations for EKI provide a qualitative insight into the essential nonlinearities responsible for the chaotic behaviour observed in EKI experiments. We emphasize that the importance of the Lorenz equations for EKI lies in their ability to capture the essence of chaotic behaviour rather than their quantitative predictions.

Acknowledgements

We acknowledge the financial support received from the Science and Engineering Research Board, Government of India, under the Mathematical Research Impact Centric Support (MATRICS) scheme (Grant No. MTR/2022/000080).

Conflicts of Interest

The authors declare no conflicts of interest.

Data Availability Statement

Data sharing is not applicable to this article as no datasets were generated or analysed during the current study

References

1. J. H. Masliyah and S. Bhattacharjee, *Electrokinetic and Colloid Transport Phenomena* (John Wiley & Sons, 2006).

2. K. Dubey, S. Sanghi, A. Gupta, and S. S. Bahga, "Electrokinetic Instability Due to Streamwise Conductivity Gradients in Microchip Electrophoresis," *Journal of Fluid Mechanics* 925 (2021): A14.

3. K. Dubey, A. Gupta, and S. S. Bahga, "Scaling Behavior in On-Chip Field-Amplified Sample Stacking," *Electrophoresis* 40, no. 5 (2019): 730–739.

4. R. Bharadwaj and J. G. Santiago, "Dynamics of Field-Amplified Sample Stacking," *Journal of Fluid Mechanics* 543 (2005): 57–92.

5. M. H. Oddy, J. G. Santiago, and J. C. Mikkelsen, "Electrokinetic Instability Micromixing," *Analytical Chemistry* 73, no. 24 (2001): 5822–5832.

6. H. Lin, "Electrokinetic Instability in Microchannel Flows: A Review," *Mechanics Research Communications* 36, no. 1 (2009): 33–38.

7. R. Gaur and S. S. Bahga, "Electrohydrodynamic Instability of Ion-Concentration Shock Wave in Electrophoresis," *Physical Review E* 95, no. 6 (2017): 063109.

8. C. C. Chang and R. J. Yang, "Electrokinetic Mixing in Microfluidic Systems," *Microfluidics and Nanofluidics* 3 (2007): 501–525.

9. S. Shin, I. Kang, and Y. K. Cho, "Mixing Enhancement by Using Electrokinetic Instability Under Time-Periodic Electric Field," *Journal of Micromechanics and Microengineering* 15, no. 3 (2004): 455.

10. J. D. Posner and J. G. Santiago, "Convective Instability of Electrokinetic Flows in a Cross-Shaped Microchannel," *Journal of Fluid Mechanics* 555 (2006): 1–42.

11. K. Dubey, A. Gupta, and S. S. Bahga, "Coherent Structures in Electrokinetic Instability With Orthogonal Conductivity Gradient and Electric Field," *Physics of Fluids* 29, no. 9 (2017): 092007.

12. P. Gupta and S. S. Bahga, "Mechanism of Sinuous and Varicose Modes in Electrokinetic Instability," *Physical Review E* 110, no. 3 (2024): 035106.

13. C. H. Chen, H. Lin, S. K. Lele, and J. G. Santiago, "Convective and Absolute Electrokinetic Instability With Conductivity Gradients," *Journal of Fluid Mechanics* 524 (2005): 263–303.

14. J. D. Posner, C. L. Pérez, and J. G. Santiago, "Electric Fields Yield Chaos in Microflows," *Proceedings of the National Academy of Sciences* 109, no. 36 (2012): 14353–14356.

15. G. Wang, F. Yang, and W. Zhao, "There Can Be Turbulence in Microfluidics at Low Reynolds Number," *Lab on a Chip* 14, no. 8 (2014): 1452–1458.

16. M. Dennin, G. Ahlers, and D. S. Cannell, "Spatiotemporal Chaos in Electroconvection," *Science* 272, no. 5260 (1996): 388–390.

17. C. Druzgalski, M. Andersen, and A. Mani, "Direct Numerical Simulation of Electroconvective Instability and Hydrodynamic Chaos Near an Ion-Selective Surface," *Physics of Fluids* 25, no. 11 (2013): 110804.

18. P. Bergé, Y. Pomeau, and C. Vidal, *Order Within Chaos* (Hermann, 1987).

19. E. N. Lorenz, "Deterministic Nonperiodic Flow," *Journal of Atmospheric Sciences* 20, no. 2 (1963): 130–141.

20. S. H. Strogatz, *Nonlinear Dynamics and Chaos: With Applications to Physics, Biology, Chemistry, and Engineering* (CRC Press, 2018).

21. Y. Guan, S. L. Brunton, and I. Novosselov, "Sparse Nonlinear Models of Chaotic Electroconvection," *Royal Society Open Science* 8, no. 8 (2021): 202367.

22. C. Sparrow, *The Lorenz Equations: Bifurcations, Chaos, and Strange Attractors*, vol. 41 (Springer New York, 1982).

23. D. Saville, "Electrohydrodynamics: The Taylor-Melcher Leaky Dielectric Model," *Annual Review of Fluid Mechanics* 29, no. 1 (1997): 27–64.

24. Q. Li, Y. Delorme, and S. H. Frankel, "Parametric Numerical Study of Electrokinetic Instability in Cross-Shaped Microchannels," *Microfluidics and Nanofluidics* 20 (2016): 1–12.

25. J. F. Hoburg and J. R. Melcher, "Internal Electrohydrodynamic Instability and Mixing of Fluids With Orthogonal Field and Conductivity Gradients," *Journal of Fluid Mechanics* 73, no. 2 (1976): 333–351.

26. S. Chandrasekhar, *Hydrodynamic and Hydromagnetic Stability* (Dover Publications, 1981).

27. N. A. Patankar, "Electrokinetic Instability: The Sharp Interface Limit," *Physics of Fluids* 23, no. 1 (2011).

28. S. Sharan, P. Gupta, and S. S. Bahga, "Mechanism of Electrohydrodynamic Instability With Collinear Conductivity Gradient and Electric Field," *Physical Review E* 95, no. 2 (2017): 023103.

29. J. C. Baygents and F. Baldessari, "Electrohydrodynamic Instability in a Thin Fluid Layer With an Electrical Conductivity Gradient," *Physics of Fluids* 10 (1998): 301–311.